ELSEVIER

Contents lists available at ScienceDirect

Computational Materials Science

journal homepage: www.elsevier.com/locate/commatsci





Multiscale Concurrent Atomistic-Continuum (CAC) modeling of multicomponent alloys

Kevin Chu^{a,*}, Adrian Diaz^b, Youping Chen^c, Ting Zhu^{a,d}, David L. McDowell^{a,d}

- ^a School of Materials Science and Engineering, Georgia Institute of Technology Atlanta, Atlanta, GA 30332, USA
- ^b X-Computational Physics Division, Los Alamos National Laboratory, P.O. Box 1663, Los Alamos, NM, USA
- ^c University of Florida, Gainesville, FL 32611, USA
- ^d Woodruff School of Mechanical Engineering, Georgia Institute of Technology, Atlanta, GA 30332, USA

ARTICLE INFO

Keywords:
Random alloys
Concurrent Atomistic-Continuum
Molecular dynamics
Average atom

ABSTRACT

Strengthening in complex multicomponent systems such as solid solution alloys is controlled primarily by the dynamic interactions between dislocation lines and heterogeneously distributed solute species. Modeling of extended defect length scales in such multicomponent systems becomes prohibitively expensive, motivating the development of reduced order approaches. This work explores the application of the Concurrent Atomistic-Continuum (CAC) method to model dislocation mobility in random alloys at extended length scales. By employing recently developed average-atom interatomic potentials, the average "bulk" material response in coarse-grained regions interacts with true random solute species in the atomistic-scale domain. We demonstrate that spurious stresses in domain resolution transition regions are eliminated entirely due to the CAC formulation. Simultaneously, the key details of local stress fluctuation due to randomness in the dislocation core region are captured, and fluctuating stress smoothly decays to the long-range dislocation stress field response. Dislocation mobility calculations, for line lengths over 400 nm, are computed as a function of alloy composition in the model FeNiCr system and compared to full molecular dynamics (MD). The results capture the composition-dependent trends, while reducing degrees of freedom by nearly 40%. This approach can be readily extended to any system described by an EAM potential and facilitates the study of large-scale defect dynamics in complex solute environments to support computational alloy design.

1. Introduction

Predictive atomistic modeling of dislocation-mediated yield and post-yield behavior of alloys has progressed significantly in recent years. Lately, attention has turned to complex multicomponent alloy systems with potentially attractive properties and new modeling challenges. To date, numerous advances have been made in modeling and simulation at multiple length scales for medium-entropy alloy (MEA) and highentropy alloy (HEA) systems [1–5]. These advances in understanding have paved the way for application of hierarchical scale bridging approaches [6] to consider larger domain sizes that sample sufficient numbers of local structures to provide understanding of mesoscopic behavior. Parameters computed from atomistic simulations can be used as inputs to reduced degree-of-freedom (DOF) models such as discrete dislocation dynamics [7–9], phase-field dislocation dynamics [10–12], or crystal plasticity models [6,13,14]. In providing such inputs,

however, the relevant aspects of the underlying physics may be lost; key details that are particularly relevant to solute strengthening in these alloys, such as chemical short range order [2], are often addressed at higher length scales using reduced order models that do not follow the trajectories of atomic reaction pathways. For example, cross-slip in allovs is not controlled by either the average or the minimum activation energy barriers among a distribution of barriers in a heterogeneous system. The rate-limiting mechanism(s) is (are) more nuanced with influences at multiple length and time scales [15]. Similarly, dislocation glide in random alloys has been shown to be line-length dependent [16,17] due to the multiple length scales of dislocation bowing and pinning/depinning at local energy minima in the potential energy surface. Analyses of both dislocation mobility and twinning-mediated deformation in homogenized "average-atom" (A-atom) simulations [2,18,19] further illustrate the strong dependence of dislocationmediated deformation on randomness in alloy DOF, resolved at

^{*} Corresponding author at: 771 Ferst Drive, Atlanta, GA 30332, USA. *E-mail address:* kchu41@gatech.edu (K. Chu).

atomistic fidelity. The accurate homogenization or simplification of numerous complex atomic-scale mechanisms into a form conducive to multiscale approaches is thus of primary importance [20].

Certain concurrent multiscale methods based on domain decomposition, on the other hand, circumvent these difficulties by explicitly computing discrete atomic values while still extending the length scale of a unified simulation system via coupling with continuum representations, for example [21]. Necessarily, the treatment of interface regions separating domains at different resolution and scale is of critical importance. Typically, coupled atomistic-continuum [22-25] modelling employs force or energy-based coupling across atomistic/continuum (A/ C) interfaces to smooth the process of coarsening spatial degrees of freedom; the continuum domain embeds average properties that may be informed or calibrated separately by prescribed atomistic calculations. The atomistic domain of the model is able to capture the nanoscale rearrangement during deformation. In recent applications to random alloys, however, such domain decomposition methods introduce spurious forces of non-negligible magnitude [26]. This exemplifies the unphysical interface modeling for the abrupt transition from true random solutes to a homogeneous material structure description in the continuum region. To address this, Nag et al. employed the A-atom embedded atom method (EAM) potential formulation [19,26] to define a "pad" region between the A/C representations. This effectively creates a buffer region in which the heterogeneous fluctuations of stress decay towards a homogeneous bulk value, smoothing the transition. However, discontinuities in stress were not eliminated, and such applications are limited by the complexity of model calibration and excessive spurious stresses due to the force or energy coupling methods.

The A-atom approach has also been applied to explicitly isolate the effect of lattice distortion and chemical short-range order in MEA [2] and to study dislocation mobility in austenitic stainless steels [18] and other HEAs [27]; this has been done by making one-to-one comparisons between single-component A-atom and true random equivalent models in atomic resolution—an "all or nothing" approach. However, the mixing of A-atom and true multicomponent solutes as explored using coupled A/C models is certainly appealing as a concurrent multiscale domain decomposition framework. Here we propose to extend the Concurrent Atomistic-Continuum (CAC) [28–31] coarse-graining approach to simulations of random alloys. CAC is a coarse-grained atomistic method. It presents a two-level atom and lattice description for a crystal as an extension of the Irving Kirkwood [32] procedure. This unified and consistent integral form finite element framework requires only a suitable interatomic potential to describe both atomic and coarsegrained resolutions, eliminating the need for ad-hoc force or energy coupling across length scale interfaces—indeed no scale interfaces exist in the domain decomposition sense. In addition, CAC utilizes a discontinuous finite element mesh that allows for long range dislocation stress fields to be preserved and transmitted [33] through coarse-grained (CG) regions, and for dislocations to propagate therein, while simultaneously reducing the system DOF. This approach has been extensively explored in recent applications, demonstrating its robustness in reproducing MD results for dislocation evolution and elucidating scale-dependent phenomena in mechanisms such as sequential dislocation slip transfer across interfaces [34]. Additionally, phonon transport behavior across the atomistic-continuum interface is reliably reproduced for multiple interfaces [35], lending confidence to treatment of highly nonequilibrium problems. Moreover, atomic mesh resolution can be employed in regions of interest using the same framework to fully resolve nanoscale defects and interactions, thereby avoiding a jump of the underlying field equations across fully resolved atomistics and coarse-grained interfaces. The net Burgers vector of each dislocation is preserved, along with the edge and screw character of partial dislocations [36].

CAC has been previously shown to preserve long-range interactions and short-range reaction characteristics, though its application has been limited to pure metals or pure metal bilayer interfaces [37]. The A-atom

approach has been validated in full MD for concurrent representation of discrete and A-atom solute types. The next consequential step is to implement the A-atom approach within CAC to enable large spatial scale simulations of random alloys, with a fully resolved atomistic domain only near reactions of interest. Recent advances in the CAC implementation have allowed for the evaluation of multicomponent EAM alloy potentials [29]. We leverage these improvements to study the influence of individual solutes on dislocation behavior in the FeNiCr ternary alloy, which is of practical relevance to austenitic stainless steels. By employing a similar A-atom approach as that of Nag et al. [26] in coarse-grained regions, we can effectively simulate dynamics in this multicomponent system without loss of detail regarding key defect-structure interactions. In the following, the A-atom approach is employed to examine static and dynamic defect behavior in heterogeneous solute fields and compared to full MD.

2. Methods

2.1. Interatomic potentials

The model system in this work is austenitic stainless steels, with nominally FeNiCr components. We employ fixed-composition EAM potentials for the ternary alloy system based on a recent FeNiCr alloy potential for stainless steels [38]. This potential is fit to both DFT and experimental data to accurately reproduce composition trends for unstable/stable stacking fault energies, elastic constants, relevant energies, and solute misfit swelling volumes. The resultant A-atom potentials are multicomponent potentials; pair interactions between true random and A-atoms are also defined. Generalized stacking fault energy curves and elastic constants have previously been derived in Chu et al. [18]. The most obvious application of this approach involves defining models at full atomic resolution that contain true random solutes in domains in which critical dislocation reactions occur, while employing A-atom in bulk regions away from these domains. This promotes faster convergence due to the smooth potential energy surface and reduces the number of degrees of freedom in the A-atom domains. This interpretation dovetails nicely with the coarse-graining approach of CAC, wherein continuum volumes and quantities embrace the A-atom average response and atomic DOF can resolve individual atom types in reaction pathway domains where the true random solute description is critical, such as the dislocation core along the dislocation line profile.

2.2. System definitions

2.2.1. Bulk A/C interfacial stress

In the CAC approach, no overlapping coupling region is required as in coupled A/C simulations, since the same governing equations apply everywhere, and no ad hoc bridging is required between atomistic and continuum domains. Thus, it is important to highlight that the label "A/ C" is a bit of a misnomer for CAC, since it is a variable resolution integral form finite element approach; however, we abide by the A/C terminology here to distinguish the fully resolved atomistic region from the CG domains to facilitate comparison with the literature. This simulation domain is set up to reproduce the dimensions employed by Nag et al. [26], as shown in Fig. 1. There are 51 lattice units in the stacking direction. Accordingly, the final cell dimensions in the x, y and z dimensions are 14.5 nm \times 14.0 nm \times 27.5 nm, oriented along $|\overline{1}12|$, [1 1 0] and $|\overline{1}1\overline{1}|$, respectively. We employ an element size in the initial bulk interface calculations that corresponds to 1728 atoms per element (APE). This size is selected to optimize the degree of coarse graining at the target system dimensions for subsequent mobility calculations. The element orientation is shown as inset in Fig. 1. Two variants of the model definition in Fig. 1 are evaluated, one in which (a) multiple planes of Aatoms are introduced in transition from the true random atomistic

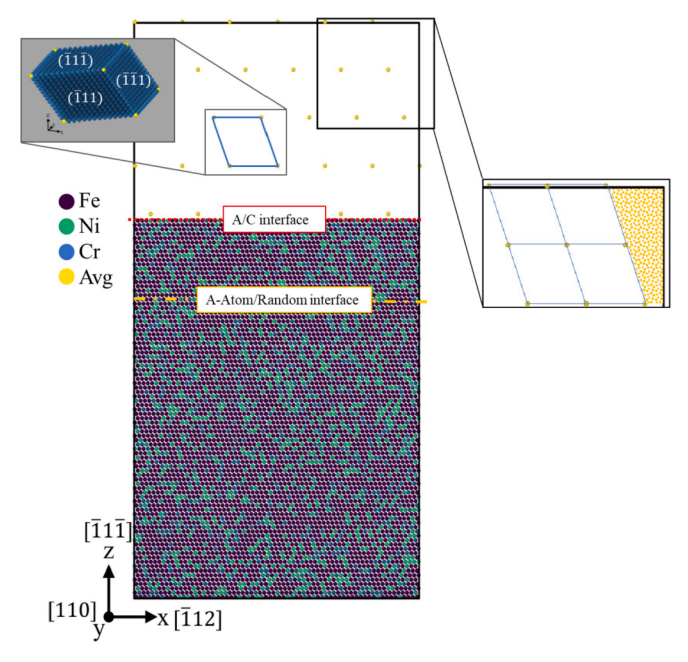


Fig. 1. Representative CAC model for evaluating bulk stress fluctuation. Approximate A/C interface (red dotted line) and A-atom interface (yellow dotdash line) are positions illustrated. Also inset is the relative finite element orientation and schematic of fill atoms at periodic boundaries. Solute types are colored according to the legend.

region as a "pad" region, and the other for which (b) the atomistic region is true random up to the A/C interface, with no pad region. All interactions in the CG regions are defined as A-atom type. Periodic boundaries are employed in the x and y directions, while the z dimension is subject to fixed free surface boundary conditions. This is similar to the standard configuration employed to calculate generalized stacking fault energies [39]. As noted in Xu et al. [33], there are still atoms present within the CG domain that correspond to "fill atoms" between elements adjacent to overall computation cell surfaces to facilitate periodic boundary conditions; these are regions in which the element faces do not coincide with the simulation cell vector—these are also set to A-atom type and are illustrated in Fig. 1. System energy is minimized via full molecular statics conjugate gradient iterations with simultaneous pressure relaxation at 0 K until the difference in total energy difference between subsequent iterations is less than 10^{-18} eV.

2.2.2. Large scale periodic dislocation configuration

The configuration of a periodic array of dislocations [40] is created by the following procedure: two halves of a crystal are stacked along the glide plane normal with the top half containing an extra plane of atoms.

Atom positions in the top and bottom halves are proportionally displaced by +/- b/2 such that the final dimensions of both crystal halves are equivalent in the glide direction (y), where b is the Burgers vector of the edge dislocation. There are 8 atomic $\left[\overline{1}1\overline{1}\right]$ planes above and below the centroid of the edge dislocation, while the remaining domain is CG. The final dimensions of the simulation cell are 400 nm \times 20 nm \times 20 nm oriented along the x, y, and z axis respectively as indicated in Fig. 3 with orthogonal orientation x = $\left[\overline{1}12\right]$, y = $\left[110\right]$, z = $\left[\overline{1}1\overline{1}\right]$. The final model contains 8,347,226 total DOF and is decomposed into 8,346,902 atoms + 324 elements (8 node elements, with 35,937 APE) while the equivalent full MD model contains 13,258,080 atoms. This equates to a DOF reduction of 37% for the CAC model. Throughout this work, DOF refers to the total number of atoms and nodes in the system.

The model is initially relaxed via molecular statics minimization using conjugate gradient descent and box dilation in the periodic dimensions (x and y) at 0 K to obtain a realistic dislocation configuration at 0 target pressure. A-atom representation is employed in this relaxation step to yield a smoother potential energy surface, reducing the risk of kinetic trapping and allowing the minimization to converge more rapidly. Following the initial full A-atom relaxation step, three separate

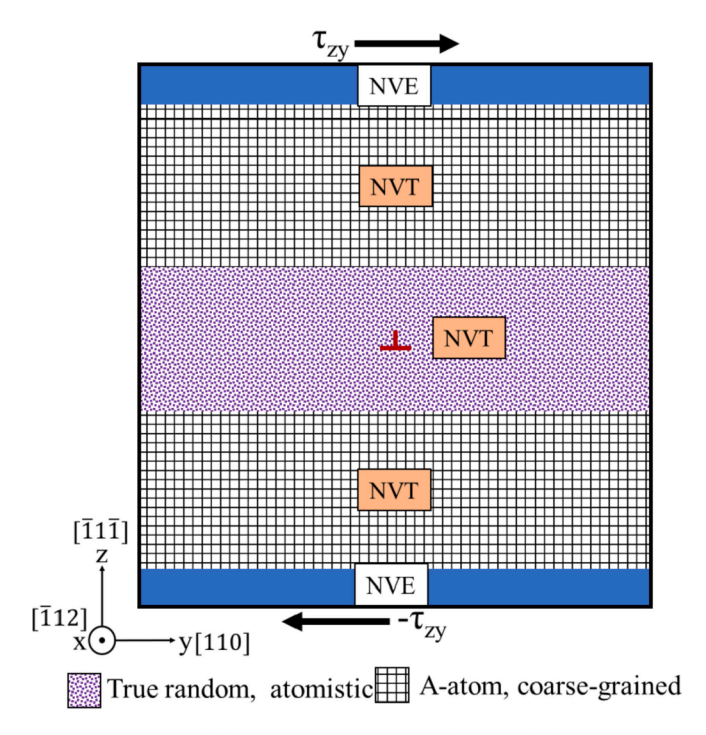


Fig. 3. Mobility model domain decomposition and ensemble definitions. Solid blue region denotes free surface boundary conditions.

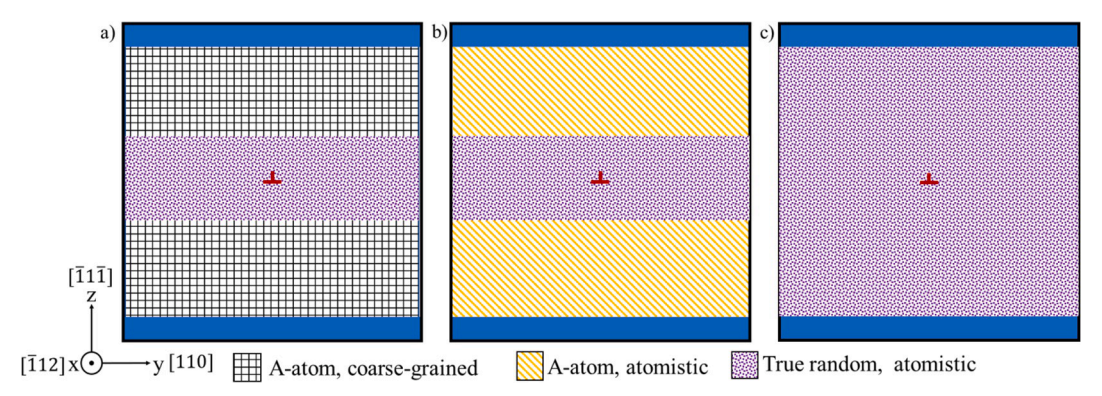


Fig. 2. Edge dislocation domain decomposition model.

domain decomposition approaches are assessed to compare quantitative accuracy of the edge dislocation stress field using molecular statics in the mixed-resolution, mixed-representation approach (Fig. 2). We employ a CAC model with no A-atom padding region (Fig. 2a), an equivalent full resolution true random and A-atom decomposed model (Fig. 2b), and a full atomistic true random alloy model (Fig. 2c). Configuration 2a is executed using CAC, while 2b and 2c are executed using LAMMPS [41]. The resultant model maintains periodicity along both the dislocation line (x) and glide direction (y), with a free surface perpendicular the z-axis. This is also referred to as a free-standing film geometry [16].

The domain decomposition described in Fig. 2a is used for dynamic CAC dislocation mobility calculations. It is worth reiterating here that a mixed A-atom (CG region)/true random (atoms) representation is employed and fully described by the mixed A-atom EAM potential—the A-atom "type" can be interpreted simply as another solute atom type. We employ the same boundary conditions as in previous full atomistic mobility studies on this system [16,18]. Periodic boundaries are applied in the dislocation glide and line directions, while free-surface boundaries are enforced in the z. Atom and nodal trajectories in the top and bottom boundary layers are solved according to NVE (constant volume and energy) ensemble, initially set to 0 K. In the interior region, a target temperature is assigned and the canonical sampling thermostat developed by Bussi et al. [42] is employed in CAC to implement the NVT (constant volume and temperature) ensemble. Per-atom forces vectors are applied to atoms in the top and bottom boundary layers as indicated in Fig. 3 to achieve the target shear stress.

The dislocation mobilities are computed at T=100~K for several applied stress levels $\tau_{zy}=50,\,100,\,150~MPa$ and Ni compositions $x_{Ni}=0.05,\,0.12,\,0.25$ for the $Fe_{70}Ni_xCr_{30-x}$ ternary alloy composition. At $x_{Ni}=0.12,\,$ the primary constituent components of 316L alloys are closely matched. The computations are repeated for three random alloy initializations at $\tau_{zy}=50,\,75,\,100,\,120,\,150~MPa.$ All simulations run for approximately 700 ps after results for the initial 6 ps are discarded. When the full dislocation line sweeps through one full periodic glide distance in the y, the top and bottom halves of the crystal are relatively displaced by one Burgers vector. Thus, we can assess dislocation displacement as the average per-atom displacement $\overline{\Delta y}$ between the top and bottom halves of the crystal in the direction of the Burgers vector b as [16], i.e.,

$$d = \frac{\overline{\Delta y}}{h} L_y \tag{1}$$

here the dislocation line is aligned along the x-axis, and the periodic glide direction with length L_y is in the y direction, as denoted in Fig. 3.

3. Results

3.1. Misfit stress fluctuations across the A/C interface

The heterogeneity in local stress fields due to swelling volume variation for solute atoms in a random alloy and their interaction with line defects is regarded as the primary source of solute strengthening [2,43,44] during glide. In addition, the influence of longer range (beyond nearest neighbor) interactions has been shown to affect predictions of more complex deformation phenomena such as cross-slip [15]. We illustrate the advantages that CAC offers compared to the coupled A/C approach in this regard by making direct comparison with the results of Nag et al. [26]. Using the configuration defined in Section 2.2.1 to isolate this variation in a defect-free system, fluctuation and subsequent dissipation of stress heterogeneities across the A/C (fully atomistic and A-Atom domains) interface are computed. Spatial binning is applied to atomic planes in the [1 1 1] stacking (z) direction, and we compute the mean and standard deviation of the per-atom virial stress; the standard deviation is plotted for all normal stress components in Fig. 4. The standard deviation of these stress components within the

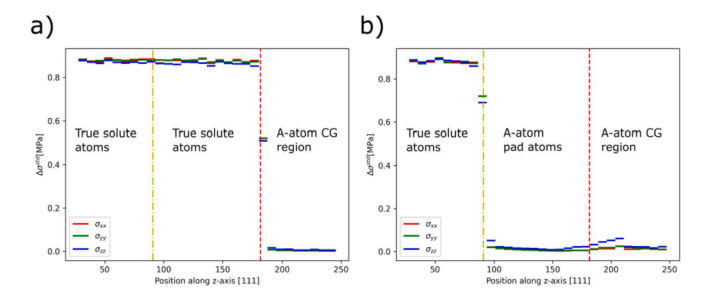


Fig. 4. Standard deviation of normal stress components for the defect-free (a) unpadded and (b) padded bulk random alloy models (2.2.1) executed using CAC. Positions of the true random/A-atom and atomistic/continuum interface as they correspond to Fig. 1 are in.

fully atomistic true random region has a magnitude of approximately 1 MPa and can be primarily attributed to the site-to-site solute misfit volume associated with true random alloy species. This fluctuation decays rapidly into the A-atom region and dissipates to 0 within $\sim 2-3$ planes in the true random/A-atom interface. Note that in Fig. 4a, the A/ C interface coincides with the random/A-atom interface, as described in Section 2.2.1. There is no distinct spike in stress that would point to discontinuity in the energetics because there is no ad-hoc coupling procedure—the true random Fe, Ni, and Cr atoms interact with A-atoms and nodes directly via the interatomic potential. For reference, the spurious stresses across the interface for a coupled A/C method was derived to be over 5 MPa for multiple alloys studied by Nag et al., spiking to nearly 40 MPa in a similar FeNiCr system to the one studied here [26]. Furthermore, it is observed that the magnitude of the stress fluctuation across the random/A-atom padding region interface (Fig. 4b) is equivalent to the fluctuation across the A/C interface representation, suggesting that there is no need for a pad region in CAC simulations using the A-atom potential; thus, a fully true random representation in the atomistic regions is used in subsequent simulations. This points to a significant advantage of the CAC method.

3.2. Dislocation stress-field fluctuation in random alloy

In addition to the local fluctuations of individual atom insertions, it is vitally important to capture the longer-range stress field of the dislocation itself. Following the configurations in Section (2.2.2), the edge dislocation stress is evaluated for a varying number of fully resolved atomic planes above and below the dislocation glide plane. The resulting stress profile across the core of a partial dislocation is plotted. The peratom virial stresses are spatially binned along the dislocation line direction (x), with a bin size of 5 $\text{Å} \times 5$ Å in the y and z directions. For all atomistic layer thicknesses, it can be observed that the stress field fluctuates in the true random solute regions, then decays smoothly into the finite element region (Fig. 5a). Slight difference in the peak stresses can be attributed to fluctuations in the partial dislocation core centroid position along the length of the wavy dislocation line (due to different random alloy instantiation) and subsequent variation in bin averages. The magnitude of stress is relatively insensitive to the number of atomic planes present; thus, the smallest of the systems is used (3.8 nm width atomistic layer thickness) to facilitate direct comparison with LAMMPS in Fig. 5b and for subsequent finite temperature mobility calculations. The local stress fluctuations present in the dislocation core profile are evident through the entire system for the fully random model, whereas the bulk stress smoothly decays to a plateau value representing the average response in the A-atom regions for both mixed resolution CAC and fully atomistic LAMMPS models (Fig. 5b). This further validates the findings in Section 3.1 that the CAC results are not affected by the absence of the padding region, and simulations executed with true random solute representation throughout the atomistic domain are equally accurate. There is agreement between CAC results and the

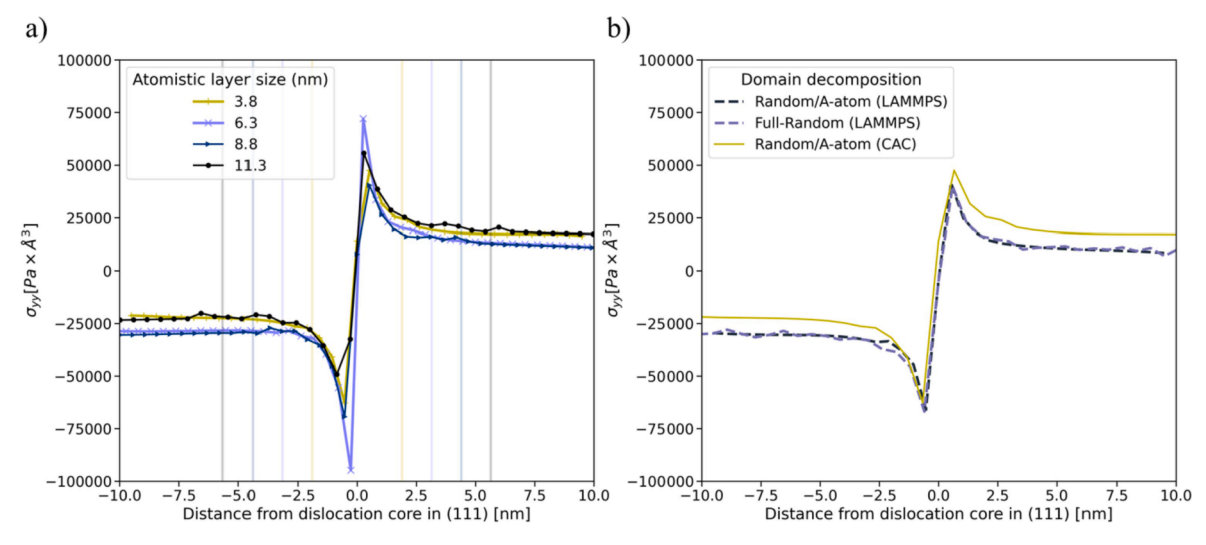


Fig. 5. σ_{yy} per-atom virial stress profile of single Shockley partial dislocation core region with a) varying thickness of fully resolved atomistic planes computed using CAC (vertical lines denote the boundary between atomistic and continuum regions) and b) comparison with LAMMPS domain decompositions as described in the text.

equivalent full atomic resolution LAMMPS model for both the mixed true random/A-atom representation and the fully random system (Fig. 5b); thus, the application of the A-atom approach within CAC can be applied robustly to simultaneously capture both the short-range fluctuations and long-range defect stress fields associated with dislocations in random alloys.

3.3. Dislocation mobility

In a single component system, dislocation glide initiates once the Peierls stress, the intrinsic lattice resistance, is overcome. In a solid solution, local barriers to dislocation motion vary spatially as a function of solute distribution [45]. This results in dislocation line bowing as it glides due to pinning/depinning at heterogeneous local obstacles. These interactions with solute misfit elastic fields form the basis of many solid solution strengthening theories [1,43,44]. As emphasized previously,

this randomness and additional source of glide resistance is vitally important to capture if an accurate mobility function is to be determined, especially for dynamic finite temperature behavior. The displacement vs. time for all target compositions and stresses are plotted in Fig. 6a, showing the run-to-run variation due to randomization of initial solute positions. The equivalent full atomistic, true random LAMMPS simulations with identical boundary conditions and thermostatting parameters are also executed at $x_{Ni} = 0.12$ (Fig. 7). Velocities at $x_{Ni} = 0.05$, 0.12 in the ternary $Fe_{70}Ni_xCr_{30-x}$ alloy are comparable, while a more significant decrease is observed at $x_{\rm Ni}=0.25$. This feature is consistent with previous simulations of screw dislocations [18]—at low temperatures (100 K) the composition dependence is no longer linear. We also notice that velocities at the lowest applied stresses (50 MPa) are negligible, indicating the presence of a minimum threshold stress required to initiate dislocation motion—another feature of glide in solid solutions that is appropriately captured by the mixed-resolution CAC

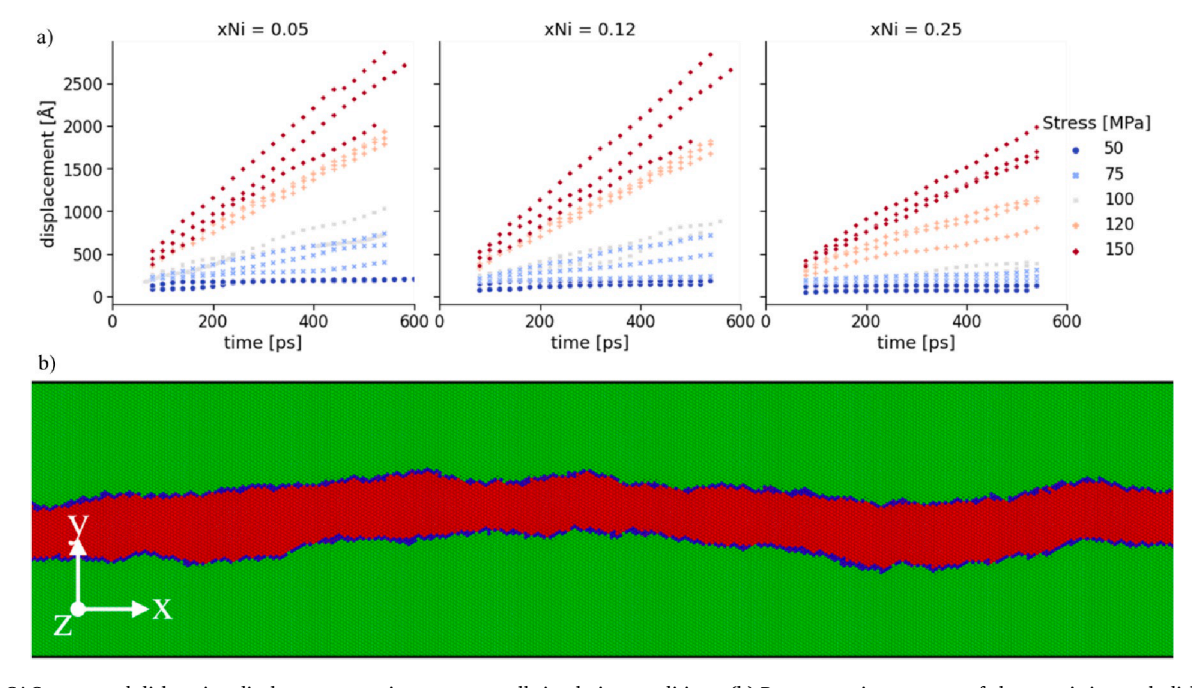


Fig. 6. (a) CAC computed dislocation displacement vs. time curves at all simulation conditions. (b) Representative segment of characteristic rough dislocation line configuration, with atoms colored by structure type (Green = FCC, Red = HCP, Blue = undetermined) as calculated by OVITO [48].

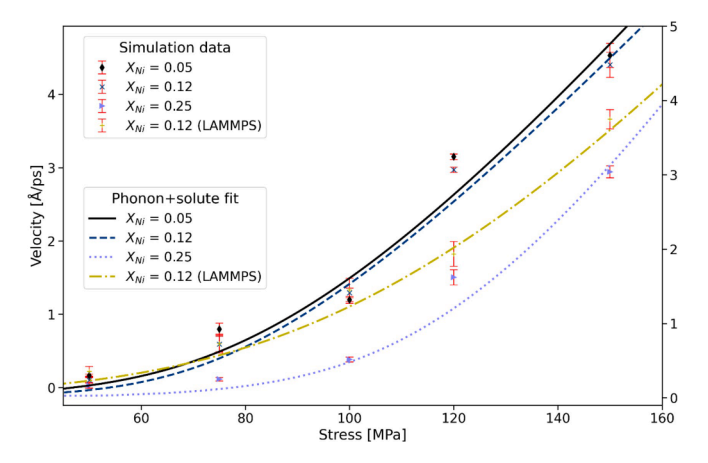


Fig. 7. Full CAC mobility results and full MD LAMMPS comparison at $x_{\rm Ni}=0.12.$ Lines denote a "phonon + solute" fit to the computed mobility functions.

simulation. This threshold "friction" stress is absent from previous A-atom simulations executed at the target alloy composition [18]. There is evidence of a low and intermediate velocity solute and phonon drag regime [46,47] for all compositions investigated here [47]. Simultaneously, the characteristic bowing associated with heterogeneously pinning solute fields in the glide plane of the dislocation are captured by the CAC/A-atom approach, evidenced by the slight run-to-run variation, and more qualitatively, the dislocation line roughness consistent with random solute fluctuation visualized in OVITO [48] (Fig. 6b). The mobility results herein are not meant to be an extensive study of dislocation mobility functions, but rather they illustrate that multiscale CAC dynamic simulations at finite temperature can indeed capture composition dependent effects and resolve the essential variation due to presence of random solute species distribution consistent with full MD results.

4. Discussion

4.1. Fitting to solute drag model

The applications of the CAC/A-atom approach to studies on dislocation behavior are laid out in the previous sections. Emphasis is placed primarily on the advantages of CAC as a concurrent multiscale modeling approach as applied to multicomponent systems; namely, there are no spurious forces in the transition between atomistic/CG resolutions even in the presence of random solute distributions in the interface region. Beyond the spatial resolution, domains are further decomposed into true random and A-atom regions. This can be interpreted as a two-level description in terms of both the length scale and influence of the distribution of chemical species. As such, CAC captures the nuanced details of large length scale dislocation glide due to the use of full atomic resolution. To illustrate this, we examine the nonlinearity of the mobility curve evident at low stresses and temperatures, indicative of the "phonon + solute" [16] drag observed in MD solid solution dislocation mobility calculations. For comparison, the drag force function recently derived by Sills et al. [16] is employed as

$$F_{ph} = Bv = CT^n v \tag{2}$$

$$F_{sol} = b\tau = b\tau_{y0} min \left\{ 1, \left(\frac{k_B T}{\Delta E_b} arsinh \left[e^{\Delta E_b/k_B T} \left(\frac{v}{2w\omega_H} \right) \right] \right) \right\}$$
 (3)

$$\tau_{drag} = \frac{F_{sol} + F_{ph}}{b} \tag{4}$$

where the fitting parameters are $B = CT^n$, τ_{y0} , ΔE_b , $w\omega_H$. Here, v is the computed dislocation velocity, b is the Burgers vector length, and k_B is Boltzmann's constant. w is a characteristic dislocation unit glide

distance and ω_H is the attempt frequency. Their product is combined into a single fitting parameter. The drag forces due to solute and phonon drag are denoted F_{sol} and F_{ph} , respectively. Our approach to fitting this function differs slightly than in Sills et al. [16] due to the additional composition parameter. Because we are comparing data at a single temperature, the "friction stress" τ_{y0} , or stress required to initiate dislocation motion at 0 K, cannot be extrapolated. Instead, we use it as a free fitting parameter and the phonon drag coefficient CT^n is collapsed into a single parameter as simply B. ΔE_h is a stress-dependent energy barrier associated with solute drag, assumed to be rate insensitive. We employ the fitting procedures implemented in SciPy [49] "optimize" package to minimize the sum of the squared residuals. Fig. 7 illustrates the resulting fit to the computed mobility data for both CAC and LAMMPS, illustrating the inflection point between the nonlinear solute drag and linear phonon drag regimes. The fitting method returned reasonable values for this cross-over point, the friction stress τ_{v0} (Table 1), based on existing MD studies [16] and critical resolved shear stress estimates from experiments [50,51]; however, all other fitting parameters $(B, \Delta E_b, w\omega_H)$ differ by approximately one order of magnitude from those in previous fits to this model [16]. The fitting parameters are provided in Table 1 below. Note that we do not modify the functional form to address solute concentration here, as CAC computations were performed for a limited number of compositions. The threshold stress determined by fitting at $x_{Ni} = 0.12$ for CAC and LAMMPS differ by ~ 18 MPa. CAC captures phonon interactions with wavelength greater than the element size [52-54], however short wavelength phonon interactions with the dislocation core cannot be captured in the coarse-grained domain. Neglecting short wavelength damping and dissipative phonon interactions with the dislocation core could reasonably lead to higher observed velocity. Moreover, the effect of thermostatting coarse-grained DOF has not been explicitly evaluated here. Thus, discrepancies in the computed mobility curve between LAMMPS and CAC may be due to the relatively large element sizes employed in these simulations, though this effect is mediated by the use of the fully resolved atomistic layers in the critical dislocation core region [35]. These simulations are executed with temperature control via the canonical sampling thermostat with velocity rescaling [42], and a more extensive study of temperature-dependent mobility is necessary to fully evaluate phonon damping effects. Lastly, Sills et al. [16] noted that they were unable to apply such a fit below 200 K to their temperaturedependent dataset due to the high threshold stress, though the range of threshold stress extracted directly from their MD dataset do match the range of our fitted results.

4.2. Temperature

The temperature definition in CAC is derived through a kinetic energy density decomposition into velocity field k_{a1} and local velocity fluctuation k_{a2} terms [28]. For an 8-node element as employed in CAC with size $n_l = V_e/V$, where V and V_e are respectively the unit cell and element volumes, the kinetic energy is given as:

Table 1 Fitting parameters for modified solute + phonon fit.

| Parameter | $	au_{y0}$ | ΔE_b | В | $w\omega_H$ |
|--------------------------|------------|--------------|--------|-------------|
| Units | MPa | eV | MPa·ps | Å/ps |
| $x_{Ni}=0.05$ | 72.73 | 0.0411 | 0.827 | 27.5 |
| $x_{Ni}=0.12$ | 74.59 | 0.0530 | 0.871 | 31.3 |
| $x_{Ni} = 0.12$ (LAMMPS) | 92.81 | 0.0332 | 1.53 | 26.3 |
| $x_{Ni}=0.25$ | 111.3 | 0.0610 | 1.26 | 20.2 |

$$\iiint_{V} k_{\alpha 1} dV + \iiint_{V} k_{\alpha 2} dV = n_{l} \times \frac{3}{2} k_{B} T$$

$$\tag{5}$$

This equivalency makes the assumption that the system is at high-temperature thermal equilibrium, allowing for the assumption that every particle DOF possesses energy $k_BT/2$. The velocity field in the element is determined from displacements $U_{\tilde{e}a}(t)$ as:

$$\widehat{v}(x,t) = S_{\xi}(x)\dot{U}_{\xi\alpha}(t) \tag{6}$$

where $S_{\xi}(x)$ is the FE shape function and $U_{\xi a}(t)$ can be interpreted as the velocity of the α -th atom embedded within the ξ -th node of the element in question—the nodal velocities, giving for the "average density" $k_{\alpha 1}$ term:

$$\iiint_{V} k_{\alpha 1}(x,t)dV = \iiint_{V} \frac{1}{2} \rho_{\alpha} \left[S_{\xi}(x) \dot{U}_{\xi \alpha} \right]^{2} dV = 8 \left(\frac{3}{2} k_{B} T \right)$$
 (7)

here, ρ_a is the contribution of the α -th atom to the mass density. The shape functions implemented in CAC are such that phonons with wavelength smaller than the element size are truncated, and the decomposition of kinetic energy density depends on the element size n_l , i.e.,

$$\iiint_{V} k_{\alpha 2}(x,t)dV = \iiint_{V} \frac{1}{2} m_{\alpha}(\widetilde{v}_{k\alpha})^{2} \overline{\delta}_{V}(x-r_{k})dV = (n_{l}-8)\left(\frac{3}{2}k_{B}T\right)$$
(8)

Representing the contribution of individual particle fluctuations $\widetilde{\nu}_{k\alpha}$ to the $k_{\alpha 2}$ kinetic energy density term.

In practice, temperature can be initialized in a straightforward manner by assigning velocities based on a Boltzmann distribution about the target average kinetic energy, in a manner similar to full atomistic simulations. While this results in a lower initial temperature in the CG regions due the absence of the local fluctuation term, the implemented thermostat effectively reaches the target kinetic energy through velocity rescaling in both the atomistic and CG regions after $\sim 6-8$ ps, depending on the timestep size. Therefore, pending a more rigorous velocity initialization implementation, this equilibration stage is crucially necessary in any finite temperature simulations with CAC. This is not a significant disadvantage, practically speaking, as finite temperature MD simulations typically involve a similar relaxation stage after initial velocity assignments. Furthermore, the fully resolved atomistic domain of interest containing the dislocation line is initialized correctly to the target temperature and dislocation reactions and fluctuations associated with mobility in this region are accurately described. The strength of the finite temperature CAC approach is that the kinetic energy and temperature evolve solely as defined by the interatomic potential (and thermostat) and T is not a separate state variable as in other multiscale methods [55]. Fig. 8 illustrates the initial temperature difference at different resolutions and subsequent evolution based on thermostat rescaling [42].

5. Conclusion

The application of the CAC method to the coarse-grained simulation of a range of multicomponent austenitic FeNiCr alloy systems has been demonstrated. By applying the average-atom representation of bulk alloy behavior with the CAC method, longer-range dislocation stress fields and dynamic response to applied stress can be effectively modeled while preserving the fully resolved atomistic details of dislocation core and line heterogeneity due to true solute representation in regions of interest. The strengths of CAC in this problem domain can be summarized as follows:

• No force or energy-coupling is required in the transition between length-scale regions; interactions are solely defined by an

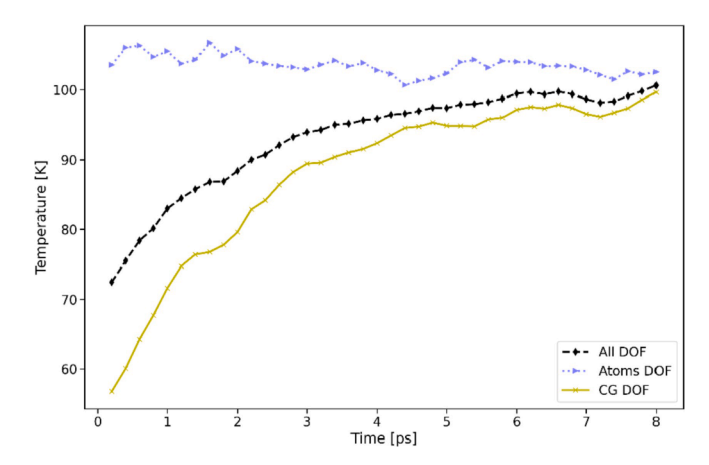


Fig. 8. Temperature control and evolution in atomistic and CG domains via temperature rescaling to target T (100 K) during equilibration step.

appropriate A-atom EAM interatomic potential, thereby eliminating spurious stresses due to true solute/A-atom discontinuity between fully resolved atomistic and coarse-grained domains common in many domain decomposition methods.

- Short-range fluctuations in stress and energy due to heterogeneous solute strain distributions are preserved. Simultaneously, long-range dislocation stress fields decay smoothly into the bulk region.
- The CAC/A-atom approach can effectively simulate the finite temperature dynamics of dislocation motion with greatly reduced number of DOF and captures composition-dependent effects such as variation of local solute energy barriers and associated dislocation line roughness when utilizing the appropriate spatial resolutions.
- Composition-dependent dislocation mobilities computed using this approach at 100 K are validated in the ternary FeNiCr system by comparing directly to equivalent full atomistic studies on edge dislocations through a "solute + phonon" fit.

These findings demonstrate that CAC with an A-atom EAM potential is an effective coarse-grained atomistic approach for the simulation of defect behavior in medium and potentially high entropy alloy systems. The ability to capture heterogenous solute-dependent effects makes this an attractive approach to apply in systems containing such fluctuations as local SRO. Further validation of temperature definition and thermostat implementation are necessary to extend applicability of this approach to relevant problems like high temperature annealing as simulated by hybrid Monte-Carlo/MD techniques. Future efforts on the development and implementation of wedge-shaped finite elements into CAC aim to eliminate the need for fill atoms along periodic boundaries, dramatically improving the already significant DOF reductions afforded by CAC.

CRediT authorship contribution statement

Kevin Chu: Writing - original draft, Writing - review & editing, Conceptualization, Investigation, Formal analysis, Visualization. Adrian Diaz: Writing - review & editing, Methodology, Software. Youping Chen: Writing - review & editing, Methodology, Supervision, Funding acquisition. Ting Zhu: Writing - review & editing, Supervision, Project administration, Funding acquisition. David L. McDowell: Writing - review & editing, Supervision, Conceptualization, Resources, Project administration, Funding acquisition.

Declaration of Competing Interest

The authors declare that they have no known competing financial interests or personal relationships that could have appeared to influence

the work reported in this paper.

Acknowledgements

K.C., T.Z., and D.L.M. acknowledge support from the Office of Naval Research under grant number N00014-18-1-2784. A.D., and Y.C. acknowledge support from National Science Foundation under grant number CMMI-176512. This work used the Hive cluster, which is supported by the National Science Foundation under grant number 1828187. This research was supported in part through research cyber-infrastrucutre resources and services provided by the Partnership for an Advanced Computing Environment (PACE) at the Georgia Institute of Technology, Atlanta, Georgia, USA.

Data availability

The processed data and input scripts required to reproduce these findings are available to download from https://github.com/kvnchv/cms2021.

References

- C. Varvenne, G.P.M. Leyson, M. Ghazisaeidi, W.A. Curtin, Solute strengthening in random alloys, Acta Mater. 124 (Feb. 2017) 660–683, https://doi.org/10.1016/j. actamat.2016.09.046.
- [2] W.R. Jian, Z. Xie, S. Xu, Y. Su, X. Yao, I.J. Beyerlein, Effects of lattice distortion and chemical short-range order on the mechanisms of deformation in medium entropy alloy CoCrNi, Acta Mater. 199 (2020) 352–369, https://doi.org/10.1016/j. actamat.2020.08.044.
- [3] E. Antillon, C. Woodward, S.I. Rao, B. Akdim, T.A. Parthasarathy, Chemical short range order strengthening in a model FCC high entropy alloy, Acta Mater. 190 (May 2020) 29–42, https://doi.org/10.1016/j.actamat.2020.02.041.
- [4] E.P. George, W.A. Curtin, C.C. Tasan, High entropy alloys: A focused review of mechanical properties and deformation mechanisms, Acta Mater. 188 (Apr. 2020) 435–474, https://doi.org/10.1016/j.actamat.2019.12.015.
- [5] S. Nag, W.A. Curtin, Effect of solute-solute interactions on strengthening of random alloys from dilute to high entropy alloys, Acta Mater. 200 (2020) 659–673, https://doi.org/10.1016/j.actamat.2020.08.011.
- [6] D.L. McDowell, Multiscale modeling of interfaces, dislocations, and dislocation field plasticity, in: CISM international centre for mechanical sciences, courses and lectures, Springer International Publishing, 2019, pp. 195–297, https://doi.org/ 10.1007/978-3-319-94186-8
- [7] H.M. Zbib, T. Diaz de la Rubia, A multiscale model of plasticity, Int. J. Plast. 18 (9) (Sep. 2002) 1133–1163, https://doi.org/10.1016/S0749-6419(01)00044-4.
- [8] J.A. El-Awady, S. Bulent Biner, N.M. Ghoniem, A self-consistent boundary element, parametric dislocation dynamics formulation of plastic flow in finite volumes, J. Mech. Phys. Solids 56 (5) (2008) 2019–2035, https://doi.org/10.1016/j. imps.2007.11.002.
- [9] E. Martínez, J. Marian, A. Arsenlis, M. Victoria, J.M. Perlado, Atomistically informed dislocation dynamics in fcc crystals, J. Mech. Phys. Solids 56 (3) (2008) 869–895, https://doi.org/10.1016/j.jmps.2007.06.014.
- [10] A. Hunter, I.J. Beyerlein, T.C. Germann, M. Koslowski, Influence of the stacking fault energy surface on partial dislocations in fcc metals with a three-dimensional phase field dislocations dynamics model, Phys. Rev. B - Condens. Matter Mater. Phys. 84 (14) (2011) 144108, https://doi.org/10.1103/PhysRevB.84.144108.
- [11] I.J. Beyerlein, A. Hunter, Understanding dislocation mechanics at the mesoscale using phase field dislocation dynamics, Philos. Trans. R. Soc. Math. Phys. Eng. Sci. 374 (2066) (2016) 20150166, https://doi.org/10.1098/rsta.2015.0166.
- [12] S. Xu, J.R. Mianroodi, A. Hunter, I.J. Beyerlein, B. Svendsen, Phase-field-based calculations of the disregistry fields of static extended dislocations in FCC metals, Phil. Mag. 99 (11) (2019) 1400–1428, https://doi.org/10.1080/ 14786435.2019.1582850.
- [13] D. L. McDowell, "Viscoplasticity of heterogeneous metallic materials," vol. 62, no. 3, pp. 67–123, 2008, doi: 10.1016/j.mser.2008.04.003.
- [14] V. Bulatov, F.F. Abraham, L. Kubin, B. Devincre, S. Yip, Connecting atomistic and mesoscale simulations of crystal plasticity, Nature 391 (6668) (1998) 669–672, https://doi.org/10.1038/35577.
- [15] W.G. Nöhring, W.A. Curtin, Cross-slip of long dislocations in FCC solid solutions, Acta Mater. 158 (Oct. 2018) 95–117, https://doi.org/10.1016/j. actamat.2018.05.027.
- [16] R.B. Sills, M.E. Foster, X.W. Zhou, Line-length-dependent dislocation mobilities in an FCC stainless steel alloy, Int. J. Plast. 135 (2020) 102791, https://doi.org/ 10.1016/j.ijplas.2020.102791.
- [17] G. Péterffy, P.D. Ispánovity, M.E. Foster, X. Zhou, R.B. Sills, Length scales and scale-free dynamics of dislocations in dense solid solutions, Mater. Theory 4 (1) (2020) 1–25, https://doi.org/10.1186/s41313-020-00023-z.
- [18] K. Chu, M.E. Foster, R.B. Sills, X. Zhou, T. Zhu, D.L. McDowell, Temperature and composition dependent screw dislocation mobility in austenitic stainless steels from large-scale molecular dynamics, NPJ Comput. Mater. 6 (1) (2020), https:// doi.org/10.1038/s41524-020-00452-x.

- [19] C. Varvenne, A. Luque, W.G. Nöhring, W.A. Curtin, Average-atom interatomic potential for random alloys, Phys. Rev. B 93 (10) (Mar. 2016), 104201, https://doi. org/10.1103/PhysRevB.93.104201.
- [20] J.H. Panchal, S.R. Kalidindi, D.L. McDowell, Key computational modeling issues in integrated computational materials engineering, CAD Comput. Aided Des. 45 (1) (Jan. 2013) 4–25, https://doi.org/10.1016/j.cad.2012.06.006.
- [21] E.B. Tadmor, R.E. Miller, Modeling materials: continuum, atomistic, and multiscale techniques, Cambridge University Press, Cambridge; New York, 2011.
- [22] S. Kohlhoff, S. Schmauder, A new method for coupled elastic-atomistic modelling, in: Atomistic simulation of materials, Springer US, 1989, pp. 411–418, https://doi. org/10.1007/978-1-4684-5703-2 42.
- [23] P.A. Klein, J.A. Zimmerman, Coupled atomistic-continuum simulations using arbitrary overlapping domains, J. Comput. Phys. 213 (1) (Mar. 2006) 86–116, https://doi.org/10.1016/j.jcp.2005.08.014.
- [24] A.V. Shapeev, Consistent energy-based atomistic/continuum coupling for two-body potentials in one and two dimensions, Multiscale Model. Simul. 9 (3) (Jul. 2011) 905–932, https://doi.org/10.1137/100792421.
- [25] J. Zhang, S. Chakraborty, and S. Ghosh, "Concurrent atomistic-continuum model for developing self-consistent elastic constitutive modeling of crystalline solids with cracks," 2, 2017. doi: 10.1615/intjmultcompeng.2017020072.
- [26] S. Nag, T. Junge, W.A. Curtin, Atomistic-continuum coupling of random alloys, Model. Simul. Mater. Sci. Eng. 27 (7) (2019), https://doi.org/10.1088/1361-651X/ab2c5c.
- [27] D. Farkas, Deformation behavior of a model high entropy alloy from atomistic simulations, Mater. Sci. Eng., A 812 (2021) 141124, https://doi.org/10.1016/j. msea.2021.141124.
- [28] Y. Chen, S. Shabanov, D.L. McDowell, Concurrent atomistic-continuum modeling of crystalline materials, J. Appl. Phys. 126 (10) (2019) 101101, https://doi.org/ 10.1063/1.5099653.
- [29] A. Diaz, "A concurrent atomistic-continuum method for massively parallel simulation of non-equilibrium solids, Doctoral Dissertation", Doctoral dissertation, University of Florida, 2020.
- [30] L. Xiong, G. Tucker, D.L. McDowell, Y. Chen, Coarse-grained atomistic simulation of dislocations, J. Mech. Phys. Solids 59 (2) (Feb. 2011) 160–177, https://doi.org/ 10.1016/j.jmps.2010.11.005.
- [31] S. Xu, T.G. Payne, H. Chen, Y. Liu, L. Xiong, Y. Chen, D.L. McDowell, PyCAC: The concurrent atomistic-continuum simulation environment, J. Mater. Res. 33 (7) (2018) 857–871, https://doi.org/10.1557/jmr.2018.8.
- [32] J.H. Irving, J.G. Kirkwood, The statistical mechanical theory of transport processes. IV. The equations of hydrodynamics, J. Chem. Phys. 18 (6) (1950) 817–829, https://doi.org/10.1063/1.1747782.
- [33] S. Xu, R. Che, L. Xiong, Y. Chen, D.L. McDowell, A quasistatic implementation of the concurrent atomistic-continuum method for FCC crystals, Int. J. Plast. 72 (2015) 91–126, https://doi.org/10.1016/j.ijplas.2015.05.007.
- [34] S. Xu, L. Xiong, Y. Chen, D.L. McDowell, Sequential slip transfer of mixed-character dislocations across σ3 coherent twin boundary in FCC metals: A concurrent atomistic-continuum study, NPJ Comput. Mater. 2 (1) (Nov. 2016) 15016, https:// doi.org/10.1038/npjcompumats.2015.16.
- [35] X. Chen, A. Diaz, L. Xiong, D.L. McDowell, Y. Chen, Passing waves from atomistic to continuum, J. Comput. Phys. 354 (Feb. 2018) 393–402, https://doi.org/ 10.1016/j.jcp.2017.10.038.
- [36] S. Xu, J. Rigelesaiyin, L. Xiong, Y. Chen, D.L. McDowell, Generalized continua concepts in coarse-graining atomistic simulations, in: Advanced structured materials, 2018, pp. 237–260, https://doi.org/10.1007/978-3-319-77504-3 12.
- [37] A. Selimov, S. Xu, Y. Chen, D. McDowell, Lattice dislocation induced misfit dislocation evolution in semi-coherent 111 bimetal interfaces, J. Mater. Res. 36 (13) (2021) 2763–2778, https://doi.org/10.1557/s43578-021-00184-8.
- [38] X.W. Zhou, M.E. Foster, R.B. Sills, An Fe-Ni-Cr embedded atom method potential for austenitic and ferritic systems, J. Comput. Chem. 39 (29) (2018) 2420–2431, https://doi.org/10.1002/jcc.v39.2910.1002/jcc.25573.
- [39] J.A. Zimmerman, H. Gao, F.F. Abraham, Generalized stacking fault energies for embedded atom FCC metals, Model. Simul. Mater. Sci. Eng. 8 (2) (Mar. 2000) 103–115, https://doi.org/10.1088/0965-0393/8/2/302.
- [40] W.-R. Jian, S. Xu, I.J. Beyerlein, On the significance of model design in atomistic calculations of the Peierls stress in Nb, Comput. Mater. Sci. (2020) 110150, https://doi.org/10.1016/j.commatsci.2020.110150.
- [41] S. Plimpton, Fast parallel algorithms for short-range molecular dynamics,
 J. Comput. Phys. 117 (1) (1995) 1–19, https://doi.org/10.1006/jcph.1995.1039.
- [42] G. Bussi, D. Donadio, M. Parrinello, Canonical sampling through velocity rescaling, J. Chem. Phys. 126 (1) (2007), https://doi.org/10.1063/1.2408420.
- [43] S. Nag, C. Varvenne, W.A. Curtin, Solute-strengthening in elastically anisotropic fcc alloys, Model. Simul. Mater. Sci. Eng. 28 (2) (2020), https://doi.org/10.1088/ 1361-651X/ab60e0.
- [44] R. Labusch, A Statistical Theory of Solid Solution Hardening, Phys. Status Solidi B 41 (2) (1970) 659–669, https://doi.org/10.1002/(ISSN)1521-395110.1002/pssb: v41:210.1002/pssb:19700410221.
- [45] E. Antillon, C. Woodward, S.I. Rao, B. Akdim, T.A. Parthasarathy, A molecular dynamics technique for determining energy landscapes as a dislocation percolates through a field of solutes, Acta Mater. 166 (Mar. 2019) 658–676, https://doi.org/ 10.1016/j.actamat.2018.12.037.
- [46] U.F. Kocks, A.S. Argon, M.F. Ashby, Thermodynamics and kinetics of slip, 1st ed., Pergamon Press, Oxford; New York, 1975.
- [47] A. Hikata, R.A. Johnson, C. Elbaum, Interaction of Dislocations with Electrons and with Phonons, Phys. Rev. B 2 (12) (Dec. 1970) 4856–4863, https://doi.org/ 10.1103/PhysRevB.2.4856.

- [48] A. Stukowski, Visualization and analysis of atomistic simulation data with OVITO-the Open Visualization Tool, Model. Simul. Mater. Sci. Eng. 18 (1) (2010) 015012, https://doi.org/10.1088/0965-0393/18/1/015012.
- [49] SciPy 1.0 Contributors, et al., SciPy 1.0: fundamental algorithms for scientific computing in Python, Nat. Meth. 17 (3) (2020) 261–272, https://doi.org/10.1038/ s41592-019-0686-2.
- [50] G. Monnet, M.A. Pouchon, Determination of the critical resolved shear stress and the friction stress in austenitic stainless steels by compression of pillars extracted from single grains, Mater. Lett. 98 (May 2013) 128–130, https://doi.org/10.1016/ j.matlet.2013.01.118.
- [51] N.Y. Juul, J. Oddershede, A. Beaudoin, K. Chatterjee, M.K.A. Koker, D. Dale, P. Shade, G. Winther, Measured resolved shear stresses and Bishop-Hill stress states in individual grains of austenitic stainless steel, Acta Mater. 141 (2017) 388–404, https://doi.org/10.1016/j.actamat.2017.09.021.
- [52] L. Xiong, D.L. McDowell, Y. Chen, Sub-THz Phonon drag on dislocations by coarse-grained atomistic simulations, Int. J. Plast. 55 (Apr. 2014) 268–278, https://doi.org/10.1016/j.ijplas.2013.11.004.
- [53] X. Chen, L. Xiong, D.L. McDowell, Y. Chen, Effects of phonons on mobility of dislocations and dislocation arrays, Scr. Mater. 137 (Aug. 2017) 22–26, https:// doi.org/10.1016/j.scriptamat.2017.04.033.
- [54] X. Chen, W. Li, A. Diaz, Y. Li, Y. Chen, D.L. McDowell, Recent progress in the concurrent atomistic-continuum method and its application in phonon transport, MRS Commun. 7 (4) (Dec. 2017) 785–797, https://doi.org/10.1557/ mrc.2017.116.
- [55] A. Diaz, D. McDowell, Y. Chen, The Limitations and Successes of Concurrent Dynamic Multiscale Modeling Methods at the Mesoscale, in: H. Altenbach, J. Pouget, M. Rousseau, B. Collet, T. Michelitsch (Eds.), Generalized Models and Non-classical Approaches in Complex Materials 2, Springer International Publishing, Cham, 2018, pp. 55–77, https://doi.org/10.1007/978-3-319-77504-3_3.